

Magnetic nanoparticles as efficient bulk pinning centers in type-II superconductors

Alexey Snezhko,^{1,*} Tanya Prozorov,^{1,2} and Ruslan Prozorov^{1,†}

¹Department of Physics & Astronomy and NanoCenter, University of South Carolina, Columbia, South Carolina 29208, USA

²School of Chemical Sciences, University of Illinois at Urbana-Champaign, Urbana, Illinois 61801, USA

(Received 28 February 2004; revised manuscript received 22 November 2004; published 28 January 2005)

Enhancement of vortex pinning by magnetic nanoparticles *embedded* into the bulk of a type-II superconductor is studied both theoretically and experimentally. Magnetic part of the pinning force associated with the interaction between a finite-size spherical magnetic inclusion and an Abrikosov vortex is calculated in the London approximation. Calculations are supported by the experimental results obtained on sonochemically modified MgB₂ superconductor with embedded magnetic Fe₂O₃ nanoparticles and compared to MgB₂ with nonmagnetic Mo₂O₅ pinning centers of similar concentration and particle size distribution. It is shown that ferromagnetic nanoparticles result in a considerable enhancement of vortex pinning in large- κ type-II superconductors.

DOI: 10.1103/PhysRevB.71.024527

PACS number(s): 74.25.-q

INTRODUCTION

Practical applications of a superconductor are determined by the maximum electric current it can carry without energy dissipation. Above first critical magnetic field, $H_{c1} = [\ln(\kappa) + 0.5]\Phi_0/(4\pi\xi^2\kappa^2)$, superconductor is filled with Abrikosov vortices.¹⁻³ Here $\Phi_0 \approx 2 \times 10^{-7}$ G cm² is the flux quantum, $\kappa = \lambda/\xi$ is the Ginsburg-Landau parameter, and λ and ξ are London penetration depth and coherence length, respectively. In high- T_c superconductors, typical values of κ are large, $\kappa > 100$, and first critical fields are small, $H_{c1} \sim 100$ Oe. In the presence of a supercurrent density \vec{j} , vortices experience a Lorentz force, $\vec{F}_L = [\vec{j} \times \vec{\Phi}_0]/c$, and, if nothing hinders their motion, accelerate until they reach viscosity-limited velocity \vec{v} . This motion creates an electric field, $\vec{E} = [\vec{B} \times \vec{v}]/c$, parallel to the current \vec{j} and, therefore, results in a finite resistivity, $\rho = E/j$. In order to prevent this dissipative process, vortices should be immobilized (pinned).¹⁻³ Pinning of vortices on structural inhomogeneities is a common way to increase critical current density. In a uniform type-II superconductor energy of a normal phase is higher by a factor of $H_c^2/(8\pi)$ per unit volume. Therefore, a vortex with the normal core of size ξ has additional energy $H_c^2\xi^2/8$ per unit length. If such vortex occupies a non-superconducting defect, part of the condensation energy is recovered and therefore this defect represents a potential well with respect to vortex displacement. Due to its origin, this is known as condensation energy or core vortex pinning. There are various ways to introduce bulk pinning centers of different nature, concentration, distribution and geometry to better utilize the condensation energy pinning (see, e.g., Refs. 1–3 for review). However, due to short coherence lengths (~ 3 – 5 nm), the pinning is weak in high- T_c superconductors.

Nonetheless, there is another possibility for the enhancement of pinning strength via direct magnetic interaction of vortices with *ferromagnetic* pinning centers. This idea was explored already in the 1960s when pinning enhancement was clearly demonstrated in low-temperature superconducting alloys with magnetic nanoparticles mechanically mixed

in.⁴⁻⁶ More recent works focused on ferromagnetic particles deposited on the surface⁷⁻¹⁰ or in the surface layer¹¹ of low-temperature superconductors. In particular, Martin *et al.* have successfully used a lattice of ferromagnetic dots (Fe or Ni) to create a periodic array of artificial magnetic pinning centers on the surface of superconducting Nb films.⁸ Moschalkov *et al.* and Van Bael *et al.* studied submicron Co particles placed on a thin Pb film and observed modulation of magnetization at low fields.^{9,10} It was concluded that periodic lattice of magnetic particles acts as an efficient 2D pinning array with pronounced matching effects. Motivated by these experiments, theoretical models of magnetic and transport responses of superconducting films with magnetic particles placed on the surface were developed.^{12,13} Although being conceptually important, these studies focused on a specific case of magnetic particle on (or close to) the surface of a thin superconducting film. The question of bulk magnetic pinning remained unexplored. In a related study, Rizzo *et al.* used ferromagnetic nanoparticles embedded in NbTi wires to achieve larger pinning strength compared to nonmagnetic Ti impurities.¹⁴ The observed enhancement was attributed to the absence of a proximity effect in magnetic metals and therefore more efficient suppression of the superconducting order parameter. However, this mechanism does not work in the case of nonmetallic pinning centers (such as oxides studied in this work) and would only be efficient for nanoparticles smaller than the coherence length (about 5 nm for MgB₂).

In this work, *bulk magnetic pinning* due to direct magnetic interaction between Abrikosov vortices and magnetic nanoparticles is studied both theoretically and experimentally. A (ferro- or ferri-) magnetic nanosized inclusion in the bulk of a type-II superconductor acts not only as a conventional core pinning center, but also gives rise to an additional magnetic component of pinning. Importantly, this is a longer-range force acting on a length scale of a penetration depth, compared to a short-range core pinning efficient at distances of the order of a coherence length. Surprisingly, there is no extended theory available yet for the description of such system. Our model consists of an infinite type-II superconductor containing an isolated straight Abrikosov vortex and a spherical magnetic particle. Pinning force associated with the

magnetic interaction between a vortex and a particle is calculated in a London approximation. Calculations are supported by the experimental results obtained on sonochemically modified MgB_2 nanocomposites with nanosized magnetic inclusions, Fe_2O_3 , and compared to a material with nonmagnetic Mo_2O_5 pinning centers of similar concentration and size distribution.

Introduction of ferromagnetic nanoparticles into the bulk of ceramics without agglomeration and/or significant phase separation is a nontrivial task. Recently, sonochemical method for modification of granular superconductors and *in situ* production of magnetic pinning centers has been developed.^{15,22} In liquid-powder slurries irradiated with high-intensity ultrasound, acoustic cavitation induces turbulent flow and shock waves. The implosive collapse of bubbles during cavitation results in extremely high local temperatures and pressures, and stimulates high-velocity collisions between suspended particles. The estimated speed of colliding particles approaches half of the speed of sound in the liquid. Effective temperatures at the point of impact can reach 3000 K, and ultrasound-caused interparticle collisions are capable of producing localized interparticle melting and “neck” formation.^{16,17} Irradiation of powdered slurries in the presence of volatile organometallics precursors produces material with nanoparticles embedded in the bulk of irradiated powders.¹⁵ In particular, sonication of MgB_2 slurry in decane with addition of small amount of $\text{Fe}(\text{CO})_5$ yields MgB_2 - Fe_2O_3 nanocomposite with significantly enhanced vortex pinning.¹⁵ Apparently, ultrasonic irradiation in the powder slurries in the presence of volatile organometallics combines the effects from both extreme cavitation hot spot and the shock waves generated in the liquid upon implosive bubble collapse.

MAGNETIC INCLUSION IN THE BULK OF TYPE-II SUPERCONDUCTOR

Let us consider a spherical magnetic particle of radius R and magnetization \vec{M} , embedded into an infinite type-II superconductor containing a single straight vortex line at the distance d from the center of the particle. This geometry is illustrated in Fig. 1, where $\vec{\Phi}_0$ indicates the direction of a magnetic field in the vortex, which carries a flux quantum Φ_0 . α is the angle between \vec{M} and $\vec{\Phi}_0$. To calculate the pinning force associated with vortex-nanoparticle interaction, distributions of magnetic induction and screening currents induced by the magnetic particle should be evaluated. We use the London equation for the vector-potential \vec{A} ($\nabla \times \vec{A} = \vec{B}$, $\nabla \cdot \vec{A} = 0$) in a superconductor:

$$\vec{\Delta} \vec{A} - \lambda^2 \vec{\Delta} \vec{A} = 0$$

and the Maxwell equations inside the magnetic particle:

$$\vec{\Delta} \vec{A} = 0.$$

Due to symmetry of the problem it is more convenient to solve the equations in spherical coordinate system (ρ, φ, θ) with the direction $\theta=0$ be parallel to the magnetization vec-

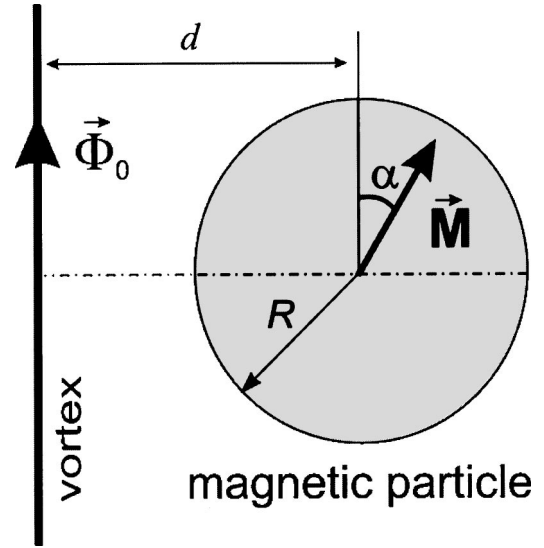


FIG. 1. Geometry of calculations: an isolated vortex at a distance d from a magnetic sphere of radius R and magnetization \vec{M} . $\vec{\Phi}_0$ indicates the direction of a magnetic field in the vortex carrying flux quantum Φ_0 .

tor \vec{M} of a particle. In this case, vector-potential \vec{A} has only one component $(0, A_\varphi(\rho, \theta), 0)$ and corresponding equations become

$$\frac{\partial^2 A_\varphi}{\partial \rho^2} + \frac{2}{\rho} \frac{\partial A_\varphi}{\partial \rho} + \frac{\cos \theta}{\rho^2 \sin \theta} \frac{\partial A_\varphi}{\partial \theta} + \frac{1}{\rho^2} \frac{\partial^2 A_\varphi}{\partial \theta^2} - A_\varphi \left(\frac{1}{\rho^2 \sin^2 \theta} + \frac{1}{\lambda^2} \right) = 0, \quad \rho \geq R,$$

$$\frac{\partial^2 A_\varphi}{\partial \rho^2} + \frac{2}{\rho} \frac{\partial A_\varphi}{\partial \rho} + \frac{\cos \theta}{\rho^2 \sin \theta} \frac{\partial A_\varphi}{\partial \theta} + \frac{1}{\rho^2} \frac{\partial^2 A_\varphi}{\partial \theta^2} - \frac{A_\varphi}{\rho^2 \sin^2 \theta} = 0, \quad \rho < R.$$

The solution should satisfy the following boundary conditions: vector potential and tangential components of the magnetic field must be continuous on the particle's surface,

$$A_\varphi^{\text{sc}}|_{r=R} = A_\varphi^{\text{m}}|_{r=R},$$

$$H_t^{\text{sc}}|_{r=R} = H_t^{\text{m}}|_{r=R} \Rightarrow (\nabla \times \vec{A}^{\text{sc}})_\theta|_{r=R} = (\nabla \times \vec{A}^{\text{m}} - 4\pi \vec{M})_\theta|_{r=R}.$$

Here m stands for the solution inside a magnetic sphere and sc denotes a superconductor. In addition, vector potential should vanish inside a superconductor at $\rho \rightarrow \infty$ and be finite inside the magnetic sphere. Then, the above equations have the following solutions:

$$A_\varphi = \frac{4\pi MR \sin \theta}{[1 + 3(\lambda/R) + 3(\lambda/R)^2]} \frac{(1 + \rho/\lambda)}{(\rho/\lambda)^2} \exp\left(-\frac{(\rho - R)}{\lambda}\right), \quad \rho \geq R,$$

$$A_\varphi = \frac{4\pi M \rho \sin \theta}{[1 + 3(\lambda/R) + 3(\lambda/R)^2]} \frac{(1 + R/\lambda)}{(R/\lambda)^2}, \quad \rho < R.$$

Corresponding screening current induced by the magnetic sphere has only one component $[0, j_\varphi(\rho, \theta), 0]$ and is calculated from the vector potential via $4\pi c^{-1} j_\varphi = (\nabla \times \vec{\mathbf{B}})_\varphi = -(\Delta \vec{\mathbf{A}})_\varphi = -A_\varphi \lambda^{-2}$. Therefore, supercurrent induced around the magnetic sphere is given by

$$j_\varphi = -\frac{cMR}{[1 + 3(\lambda/R) + 3(\lambda/R)^2]} \frac{(1 + \rho/\lambda)}{\rho^2} \exp\left(-\frac{\rho-R}{\lambda}\right) \sin \theta.$$

Let us now calculate the pinning force associated with the magnetic interaction between a magnetic sphere and a vortex. Assuming that vortex is positioned at a distance d from the particle, the corresponding interaction force is found from

$$\vec{\mathbf{F}}_{mag} = c^{-1} \int [\vec{\mathbf{j}}(\rho_v, \theta_v) \times \vec{\Phi}_0] dl,$$

where dl is a flux line element, c is the speed of light, $\vec{\mathbf{j}}(\rho_v, \theta_v)$ is the supercurrent density at the location of the vortex core, and the integration is carried over the entire vortex length. Evidently, the resulting force is attractive and maximal when particle's magnetization and magnetic field of a vortex are collinear. Analysis of the calculated pinning force shows that for $\rho - R > \lambda$ the magnetic pinning force is $f_{mag} \sim \exp[-(\rho - R)/\lambda]$. Therefore, magnetic pinning force has much larger action radius, λ , compared to the core pinning force, which acts at distances of ξ . In the general case of an arbitrary orientation, the value of magnetic pinning force is scaled by the factor of $\cos(\alpha)$, where α is the angle of misalignment. In addition, the vortex is experiencing additional moment of forces which is trying to align it along the magnetic moment of the sphere. The magnitude of this moment of forces, K , acting on the vortex line with respect to the point where vortex crosses the $\theta = \pi/2$ plane is given by

$$K = 2M\Phi_0 R \sin(\alpha) \frac{\exp\left(\frac{R}{\lambda}\right)}{1 + 3(\lambda/R) + 3(\lambda/R)^2} P\left(\frac{d}{\lambda}\right),$$

$$P\left(\frac{d}{\lambda}\right) = \int_{d/\lambda}^{\infty} (1+x)x^{-2} \sqrt{x^2 - \left(\frac{d}{\lambda}\right)^2} \exp(-x) dx.$$

Calculated magnetic pinning force acting on the flux line placed near the magnetic spherical particle is shown in Fig. 2 for different particle radii. The Ginsburg-Landau parameter, $k = \lambda/\xi$, was chosen to be 100 in our calculations. The evolution of the moment of forces acting on the vortex due to misalignment with the magnetization vector of particle is presented in the inset as a function of the distance between vortex and particle. For angles $\pi/2 < \alpha < \pi$, magnetic pinning force becomes repulsive. However, for a large number of nanoparticles randomly distributed in the bulk of a superconductor, even repulsive forces leads to an enhancement of the bulk pinning force.¹⁻³ Also, for smaller particles magnetization vector will always be aligned along the vortex direction, thus providing overall enhancement of the bulk pinning force.

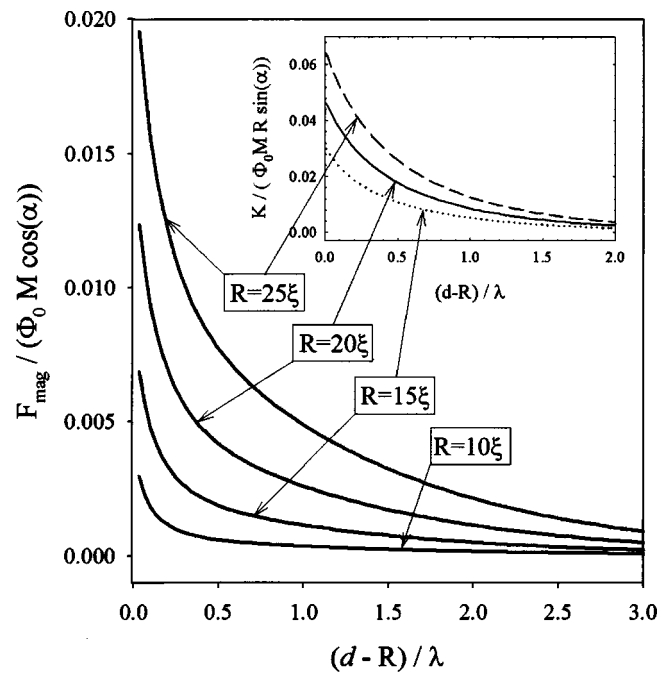


FIG. 2. Magnetic pinning force as a function of the distance between a vortex and a magnetic sphere calculated for different sphere radiuses for $\kappa=100$. Inset: Variation of the moment of forces, K , with the vortex-particle distance for different particle's radiuses.

EXPERIMENT

Detailed description of ultrasonic modification of MgB_2 and sonochemical preparation of $\text{MgB}_2\text{-Fe}_2\text{O}_3$ superconductor-ferromagnet nanocomposites has been reported elsewhere.¹⁵ In brief, 2 wt. % slurry of MgB_2 polycrystalline powder (325 mesh, Alfa Aesar) in 15 ml of decalin was irradiated with ultrasound at 20 kHz and $\sim 50 \text{ W/cm}^2$ under the ambient atmosphere, using direct-immersion ultrasonic horn (Sonics VCX-750). $\text{MgB}_2\text{-Fe}_2\text{O}_3$ nanocomposites were prepared by sonochemical irradiation of 2 wt. % MgB_2 slurry with the addition of 0.5 mmol $\text{Fe}(\text{CO})_5$, 0.9 mmol $\text{Fe}(\text{CO})_5$, and 1.8 mmol $\text{Fe}(\text{CO})_5$, respectively.¹⁸ $\text{MgB}_2\text{-Mo}_2\text{O}_5$ nanocomposites were prepared by sonochemical irradiation of 2 wt. % MgB_2 slurry with the addition of 0.5 mmol $\text{Mo}(\text{CO})_6$, 0.9 mmol $\text{Mo}(\text{CO})_6$, and 1.8 mmol $\text{Mo}(\text{CO})_6$, respectively.^{19,20} The resulting materials were filtered, washed repeatedly with pentane, and air-dried overnight. No postsynthetic sintering was performed, since ultrasonic treatment affects the morphology and leads to modification of the optimal sintering protocols. Moreover, it modifies the intergrain coupling,¹⁵ which affects measured magnetic response. Being additive to the effect of embedded nanoparticles this would complicate the data analysis. Equal molar equivalents of $\text{Fe}(\text{CO})_5$ or $\text{Mo}(\text{CO})_6$ were added in each case, therefore sonochemical synthesis was expected to yield similar number and size distribution of in-situ produced nanoparticles.²¹ Scanning electron microscopy study was conducted on Hitachi S-4700 instrument. Average size of granules obtained after irradiation of MgB_2 slurry with high-intensity ultrasound, was found to be

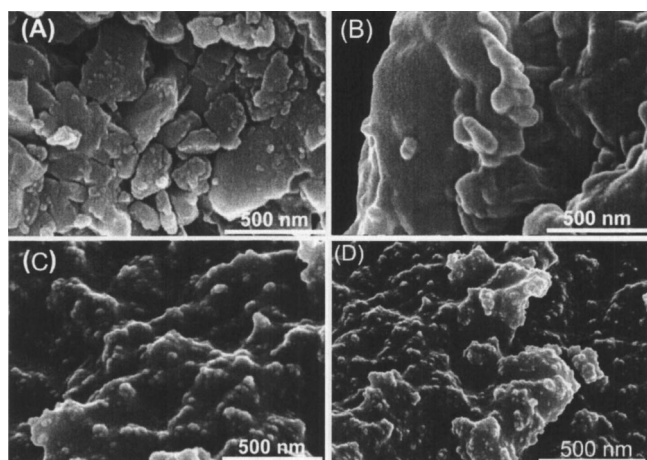


FIG. 3. Sonochemical modification of MgB_2 superconductor: (A) Starting material. (B) MgB_2 irradiated with high-intensity ultrasound. (C) MgB_2 sonicated with 1.8 mmol $\text{Fe}(\text{CO})_5$. (D) MgB_2 sonicated with 1.8 mmol $\text{Mo}(\text{CO})_6$; sonication was performed in 2% (w/w) decalin slurry at 263 K, 20 kHz, and $\sim 50 \text{ W}/\text{cm}^2$.

$\sim 30 \mu\text{m}$. Samples were additionally characterized by powder x-ray diffraction. Figure 3 shows SEM images of (A) polycrystalline MgB_2 before sonication, (B) MgB_2 irradiated with high-intensity ultrasound, (C) MgB_2 sonicated with $\text{Fe}(\text{CO})_5$, which is believed to produce a nanocomposite material with Fe_2O_3 nanoparticles,^{18,21} and (D) MgB_2 sonicated with $\text{Mo}(\text{CO})_6$ —resulted, presumably, in embedded Mo_2O_5 nanoparticles.^{19,20} No nanoparticles were formed in MgB_2 sonicated without any organometallic compounds. In contrast, sonication of granular MgB_2 in the presence of volatile organometallic compounds allows formation of nanoparticles (brighter $\sim 50 \text{ nm}$ spots easily visible in the last two pictures). In order to verify that these are, indeed, nanoparticles obtained *in situ*, the localized energy dispersive x-ray analysis (EDX) was conducted on these materials, using both scan mode and spot mode. The normalized spectrum obtained on a sonicated material is shown in Fig. 4(a). No change in the main Mg line is observed, while a small oxygen peak appears because sonication is carried out under the ambient atmosphere. Figure 4(b) shows significant changes in the spectra after introduction of iron pentacarbonyl, which results in Fe_2O_3 nanoparticles. In the spectra measured “off-spot,” the relative content of iron with respect to magnesium is nearly zero. The situation is opposite for the “on-spot” measurement. There, iron oxide with the nominal chemical composition of $\text{Fe}_{1.8}\text{O}_{3.1}$ is detected. Similar results are obtained for the nanocomposites containing Mo_2O_5 nanoparticles. Figure 4(c) indicates presence of molybdenum oxide particles with the nominal chemical composition of $\text{Mo}_{1.9}\text{O}_{4.9}$. Composition of metal oxide nanoparticles determined with EDX measurements essentially matches the stoichiometric composition of iron and molybdenum oxides, Fe_2O_3 and Mo_2O_5 . Minute traces of titanium [only visible in Fig. 4(a)] are due to the erosion of Ti horn caused by the abrasive action of suspended MgB_2 grains during the ultrasonic irradiation of decalin slurries.

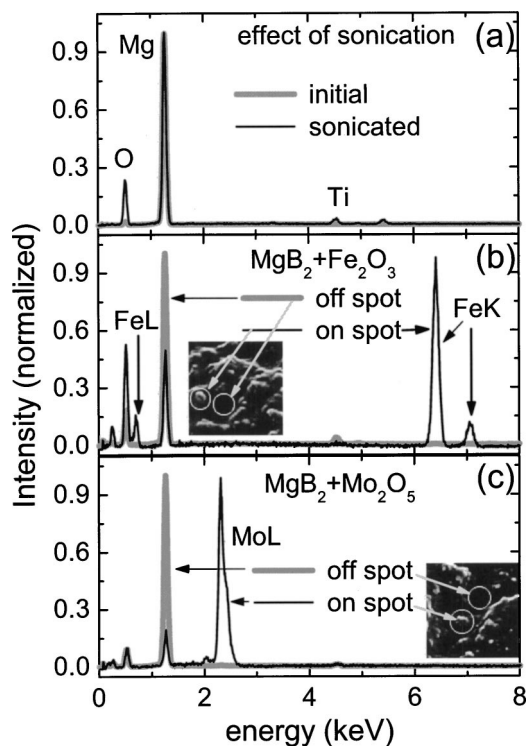


FIG. 4. Local energy dispersive x-ray spectroscopy (EDX) obtained in (a) sonicated material, (b) sonicated MgB_2 with embedded Fe_2O_3 nanoparticles, and (c) MgB_2 with embedded Mo_2O_5 nanoparticles. The “on-spot” and “off-spot” locations and corresponding spectra are indicated in the insets.

Magnetic measurements were conducted using a *Quantum Design* superconducting quantum interference device (SQUID) MPMS magnetometer. The average sample mass was maintained 10 mg. Measured magnetic moment was normalized using the initial slope, dM/dH . This slope is proportional to the volume of the superconducting phase, and for materials without magnetic nanoparticles such normalization eliminates the contribution of the demagnetization factor and gives the volume magnetization. For composites containing Fe_2O_3 nanoparticles, the normalization was done after subtraction of the paramagnetic contribution measured above T_c , which however was almost negligible. Figure 5 shows magnetization loops measured at 5 K in three studied samples: MgB_2 (sonicated, no additives); MgB_2 containing Fe_2O_3 nanoparticles [obtained by sonication with $\text{Fe}(\text{CO})_5$]; and MgB_2 with nonmagnetic Mo_2O_5 nanoparticles [obtained by sonication with $\text{Mo}(\text{CO})_6$]. As expected, magnetization loops for MgB_2 with nanosized inclusions are more hysteretic compared to the material without inclusions, which implies enhanced pinning strength. Furthermore, the loop measured in the material with magnetic Fe_2O_3 is significantly more hysteretic.

Quantitative analysis of the critical current density in the case of granular superconductors is difficult. However, it is possible to estimate its value by assuming a collection of decoupled grains. In the practical units (cgs, but current density in A/cm^2), the current density j_c is related to the irreversible magnetization M [emu/cc] via $j_c = 30M/w$, where

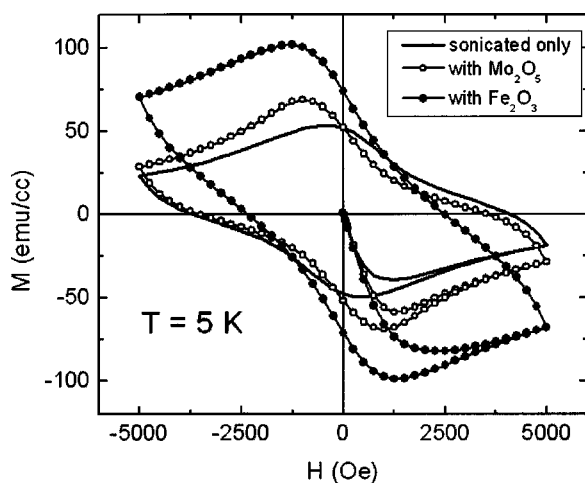


FIG. 5. Magnetization loops for the reference sample (solid line), Mo_2O_5 -containing composites (open symbols), and Fe_2O_3 -containing composites (solid symbols).

square grains of planar size $2w \times 2w$ are assumed. From the data of Fig. 5, $M \approx 50$ emu/cc for a sonicated material without nanoparticle inclusions. With $w = 15 \mu\text{m}$ we obtain $j_c = 1 \times 10^6$ A/cm², in a good agreement with the literature. In a sample with Fe_2O_3 inclusions this number is doubled indicating a significant effect of the magnetic pinning. To provide a visual representation of the temperature dependence of a critical current, magnetization data collected after zero field cooling and application of a 1 kOe magnetic field were converted into j_c and the result is shown in Fig. 6. Clearly, the enhancement is observed in the entire temperature range. It should be noted that superconducting transition temperature

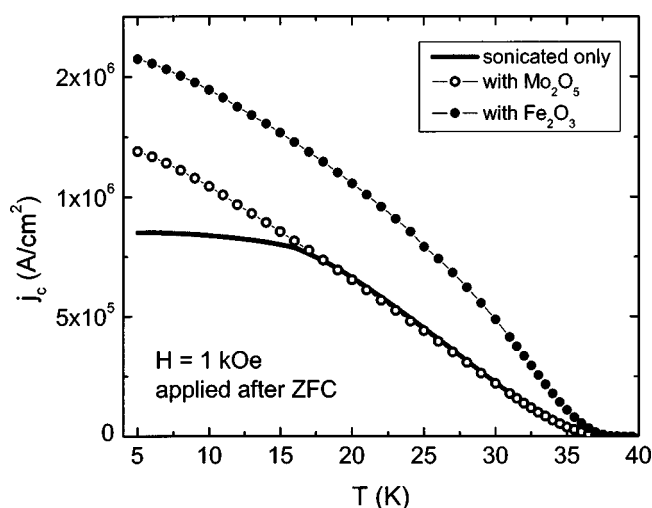


FIG. 6. Temperature dependence of the critical current density calculated from the Bean model as described in the text. The original magnetization curves were measured on warming upon application of a 1 kOe magnetic field after cooling in a zero magnetic field. Solid line is the reference sample; open symbols show Mo_2O_5 -containing nanocomposite; full symbols show nanocomposite with Fe_2O_3 nanoparticles.

did not change after the sonochemical treatment as evident from Fig. 6. This indicates that magnetic component does not act as a dopant (in which case magnetic ions would suppress T_c), but forms well shaped inclusions, also observed by SEM and TEM and confirmed by EDX, Fig. 4. Similar magnetic behavior was observed for other concentrations of embedded nanoparticles. Comparing the samples with nonmagnetic and magnetic pinning centers, we conclude that magnetic nanoparticles lead to a considerable increase of the total bulk pinning force.

Another important conclusion is that magnetic pinning is more efficient in high- κ high- T_c superconductors compared to low- κ low- T_c superconductors. This is because the energy of a vortex in type-II superconductor can be written as $E_v \approx (\Phi_0/4\pi\lambda)^2(\ln \kappa + 0.5)$, where additional factor 0.5 to $\ln \kappa$ comes from the contribution of the vortex core.³ For low- κ superconductors, core-energy term is dominant or comparable to the magnetic term. Consequently, lowering the magnetic energy by interaction with a magnetic inclusion does not significantly affect total vortex energy. As a result, the effectiveness of magnetic pinning is relatively low. The situation is opposite in high- κ materials, such as high-temperature superconductors where magnetic term is dominant and minimization of the magnetic vortex energy significantly lowers its total energy resulting in higher effectiveness of pinning associated with the magnetic interaction. Another interesting aspect of magnetic pinning is its dependence on the angle between the direction of magnetization in nanoparticles and the flux lines. Oriented nanocomposite materials should have anisotropic pinning enhancement. The experimental work on oriented nanocomposites is in progress.

CONCLUSIONS

In conclusion, it is shown that magnetic pinning force is a long-range force with a characteristic length λ . The magnitude of this force depends on the magnetization value, particle size and orientation of the magnetization vector in the magnetic particle with respect to the orientation of a flux line. The experiments with MgB_2 superconductor treated with high-intensity ultrasound have confirmed the theory—considerable improvement of a magnetic hysteresis was observed in samples with embedded magnetic Fe_2O_3 nanoparticles compared to a material with nonmagnetic Mo_2O_5 of similar concentration and size distribution. Our results suggest a new direction in the improvement of vortex pinning in high- T_c superconductors.

ACKNOWLEDGMENTS

Discussions with Yu. Genenko, B. Ivlev, V. Geshkenbein, K. S. Suslick, A. Polyanskii, and A. Gurevich are greatly appreciated. This work is supported by the NSF-EPSCoR Grant EPS-0296165, a grant from the University of South Carolina Research and Productive Scholarship Fund, and the donors of the American Chemical Society Petroleum Research Fund. The SEM study was carried out in the Center for Microanalysis of Materials (UIUC), which is partially supported by the DOE under Grant DEFGO2-91-ER45439.

*Present address: Materials Science Division, Argonne National Laboratory, Argonne, IL 60439.

†Corresponding author. Email address: prozorov@sc.edu. FAX: 803-777-3065.

- ¹A. M. Campbell and J. E. Evetts, *Critical Currents in Superconductors* (Taylor & Francis Ltd., London, 1972).
- ²G. Blatter, M. V. Feigelman, V. B. Geshkenbein, A. I. Larkin, and V. M. Vinokur, *Rev. Mod. Phys.* **66**, 1125 (1994).
- ³E. H. Brandt, *Rep. Prog. Phys.* **58**, 1465 (1995).
- ⁴D. Brochier, P. Cardinne, and M. Renard, *J. Phys. (Paris)* **29**, 953 (1968).
- ⁵T. H. Alden and J. D. Livingston, *J. Appl. Phys.* **37**, 3551 (1966).
- ⁶C. C. Koch and G. R. Love, *J. Appl. Phys.* **40**, 3582 (1966).
- ⁷P. N. Togulev, V. V. Bazarov, I. B. Khaibullin, and N. M. Suleimanov, *Low Temp. Phys.* **28**, 250 (2002).
- ⁸J. I. Martin, M. Velez, J. Nogues, and I. K. Schuller, *Phys. Rev. Lett.* **79**, 1929 (1997).
- ⁹V. V. Moschalkov, M. Baert, V. V. Metlushko, E. Rosseel, M. J. Van Bael, K. Temst, Y. Bruynseraede, and R. Jonckheere, *Phys. Rev. B* **57**, 3615 (1998).
- ¹⁰M. J. Van Bael, K. Temst, V. V. Moschalkov, and Y. Bruynseraede, *Phys. Rev. B* **59**, 14 674 (1999).
- ¹¹D. J. Morgan and J. B. Ketterson, *Phys. Rev. Lett.* **80**, 3614 (1998).
- ¹²M. V. Milosevic, S. V. Yampolskii, and F. M. Peeters, *Phys. Rev. B* **66**, 174519 (2002); M. V. Milosevic and F. M. Peeters, *ibid.* **68**, 094510 (2003).
- ¹³I. F. Lyuksyutov and V. Pokrovsky, *Phys. Rev. Lett.* **81**, 2344 (1998).
- ¹⁴N. D. Rizzo, J. Q. Wang, D. E. Prober, L. R. Motowidlo, and B. A. Zeitlin, *Appl. Phys. Lett.* **69**, 2285 (1996).
- ¹⁵T. Prozorov, R. Prozorov, A. Snezhko, and K. S. Suslick, *Appl. Phys. Lett.* **83**, 2019 (2003).
- ¹⁶K. S. Suslick, *MRS Bull.* **20**, 29 (1995).
- ¹⁷K. S. Suslick and S. J. Doctycz, *Science* **247**, 1067 (1990).
- ¹⁸X. Cao, R. Prozorov, Y. Koltypin, G. Kataby, I. Felner, and A. Gedanken, *J. Mater. Res.* **12**, 402 (1997).
- ¹⁹N. A. Dhas and A. Gedanken, *Chem. Mater.* **9**, 3144 (1997).
- ²⁰N. A. Dhas and A. Gedanken, *J. Phys. Chem. B* **101**, 9495 (1997).
- ²¹X. Cao, Y. Koltypin, R. Prozorov, G. Kataby, and A. Gedanken, *J. Mater. Chem.* **7**, 2447 (1997).
- ²²T. Prozorov, B. McCarty, Zh. Cai, R. Prozorov, and K. S. Suslick, *Appl. Phys. Lett.* **85**, 3513 (2004).